

¹ Institute of Geophysics and Meteorology, University of Cologne, Germany

² CSIRO Earth Observation Centre, Canberra, ACT, Australia

Simulating evapotranspiration in a semi-arid environment

H. Hübener¹, M. Schmidt², M. Sogalla¹, and M. Kerschgens¹

With 8 Figures

Received October 2, 2003; accepted February 16, 2004

Published online December 15, 2004 © Springer-Verlag 2004

Summary

In this work, simulations with the mesoscale meteorological model FOOT3DK for a semi-arid research site in southern Morocco are presented. The main aim of this study is to introduce two different ways to improve the soil moisture distribution towards a more realistic pattern. One of them resembles the availability of groundwater resources below the lower boundary of the soil part of the model, the other one resembles irrigation practices in the region. Additionally, we introduce a newly derived land use/land cover data set obtained from analysis of LANDSAT data and compare the simulation results to those obtained with the USGS GLCC data. To evaluate the results with the refinements in soil moisture and land use/land cover, we focus on evapotranspiration, as the quantity which is most tentative to the changes in soil moisture and is an important part of the local hydrological cycle. To evaluate the importance of sub-grid scale surface heterogeneity in soil moisture and land use/land cover, we present simulations with enhanced surface resolution. Simulation results are compared to point measurements at different sites in the research area for validation.

The results show, that a deep groundwater table and irrigation of parts of the research area can be represented by the methods we used. Simulated transpiration is overestimated compared to measured values, but this is due to the maximum approach used in this work. Finer tuning of the artificial enhancement of soil moisture with the two methods presented here are expected to lead to realistic distributions of evapotranspiration and related quantities, therewith drastically enhancing simulation accuracy for this site. As uncertainties of soil moisture distribution and restricted representation of soil moisture dynamics in meteorological models is a common problem especially for arid and semi-

arid sites, we expect our results to be useful for meteorological simulations in other arid or semi-arid areas as well.

1. Introduction

Semi-arid regions, as southern Morocco, experience high interannual variability of the scarce rainfall distribution and are most vulnerable to climatic changes. This is likewise true for changes in land use, population density and other factors, that determine water demand (Gleick, 1992; Bullock and Le Houérou, 1996). Those regions of the world bear a remarkable amount of biodiversity: in Morocco 4500 different plants are found including 600 endemic and 194 threatened species (Solh et al., 2001). Average annual rainfall determines production of biomass, thus affecting the capacity for animal production (Le Houérou and Hoste, 1977). Consequences of climate change are expected to be of crucial importance for livestock, fruit production and tourism in the High Atlas region (Parish and Funnell, 1999). Against this background, enhanced interannual rainfall variability as deduced by Hulme (1992) for the region south of the High Atlas implies enhanced vulnerability.

The work presented here is embedded in the research project IMPETUS (Ein Integratives Management Projekt für den Effektiven und

Tragfähigen Umgang mit der Ressource Süßwasser in West-Africa). Employing an interdisciplinary approach, IMPETUS aims at solution strategies for the management of scarce fresh water resources in West Africa. The project focuses on two river catchments representative for the latitude belts north and south of the Saharan desert. In these catchments, water availability, quality and sustainability are investigated. The Ouémé catchment is located in Benin and the Drâa catchment in southern Morocco. Only the latter will be discussed in this paper.

A meteorological model chain is employed for downscaling meteorological information in order to understand the atmospheric branch of the hydrological cycle in the area. At the high-resolution end of this model chain, the non-hydrostatic mesoscale model FOOT3DK (**Flow Over Orographically structured Terrain, 3 Dimensional, Köln Version**) is used for meteorological simulation. The aim is to specify the amount of water vapour induced into the local atmosphere via evaporation and plant transpiration (also referred to as evapotranspiration), for it is assumed to be one of the major fresh water sinks in the region.

As often meteorological measurements for semi-arid regions are not available or very sparsely distributed, a different approach is needed there. Several authors have used remote sensing methods to obtain meteorological near surface values, and especially surface energy fluxes (e.g. Kustas et al., 1991; Kite and Droogers, 2000). They refer to significant differences in latent heat flux due to different methods of measurement or calculation. Especially when spatial values are needed, estimation becomes very difficult.

Therefore, simulating evapotranspiration with Soil-Vegetation-Atmosphere Transfer (SVAT) schemes is an approach often used when spatial data of this quantity are needed. However, the outcome depends on the model and the parameterisations, as well as on resolution and representation of surface properties. Simulation of the surface energy budget for the HAPEX-Sahel region with a mesoscale model revealed considerable spatial variability in surface fluxes due to the associated differences of soil moisture (Taylor et al., 1997). Surface energy exchange

was also simulated for a semi-arid site in Oklahoma and validated with a wide variety of ground measurements (Brotzge and Weber, 2002). There, soil type, vegetation structure and roughness length are found to influence surface fluxes substantially. Braun et al. (2001) conducted a study for a research site in western Germany with the Lokal Modell (LM) of the German Weather Service (DWD). This model has similar soil physics as FOOT3DK. They artificially enhanced soil moisture by 50% and 100% to tune the model to measurements. This improved the representation of sensible and latent heat fluxes but reduced the heating of the boundary layer, leading to underestimation of daily maximum temperature. Two other methods of artificially enhancing soil moisture content will be described and discussed in this paper.

Recent works point out the importance of the influence of sub-grid surface heterogeneity on surface energy fluxes and boundary layer properties (cf. Shao et al., 2001). Besides the well-known aggregation effect, Shao et al. (2001) also find a dynamic effect, which is due to turbulent sub-grid motions induced by sub-grid surface heterogeneity. The dynamic effect leads to underestimation of turbulent kinetic energy (tke) for coarser resolutions and calls for a revised parameterisation of tke in the model. An improved tke parameterisation, resulting from their work is implemented in the FOOT3DK version used in this study.

Verification of simulation results is difficult, as already pointed out above. We will use some upscaled point measurements to validate the results of our study. The question of uncertainties resulting from upscaling transpiration measurements in time and space are discussed by Infante et al. (1997).

The objective of this work is to develop a simple method to improve meteorological simulation of evapotranspiration and related quantities in a semi-arid environment. In order to cope with scarce input data and the limitations of the soil model, artificial soil moisture distributions are implemented using reasonable assumptions on soil moisture distribution in the area. Additionally, a newly derived land use/land cover data set for the catchment is introduced and its benefits for the simulations are presented. The results show, that in data-sparse regions simulations

can yield plausible and consistent fields of surface energy budget components, even when only limited input data are available.

2. Investigation area

The Drâa catchment (thin black outline in Fig. 1a) reaches from the southern slopes of the High Atlas to the Saharan desert, where the river dries out. The simulation area covers the middle part of the catchment, where the Drâa oasis extends into the desert (square in Fig. 1a). Topography and vegetation coverage of the model area are depicted in Fig. 1b.

Locations of IMPETUS measurement stations are indicated by black triangles. Name, geographical position and elevation above sea level are given in Table 1.

The region is characterised by complex and in some locations steep orography, and by sparse vegetation cover apart from the Drâa oasis. The

southern slopes of the High Atlas feed the river and water is stored in an artificial lake near the city of Ouarzazate. Part of this water is distributed for daily use in the city of Ouarzazate and the wadi. Additionally, two to five times a year, depending on the water level of the lake, a large amount of water (several 1.000.000 m³, called 'laché') is used to produce hydropower and poured into the irrigation system of the wadi. This water is distributed in a system of canals for short time flooding of the date palm gardens (*Phoenix dactylifera*). Outside the oasis vegetation consists mainly of scattered *Acacia*, *Tamarix* and *Ziziphus* plants (Finckh and Staudinger, 2002).

3. Relevant aspects of the model physics and data sets

FOOT3DK is a prognostic mesoscale meteorological model, originally derived for use in mid-latitudes. Details of the model and further

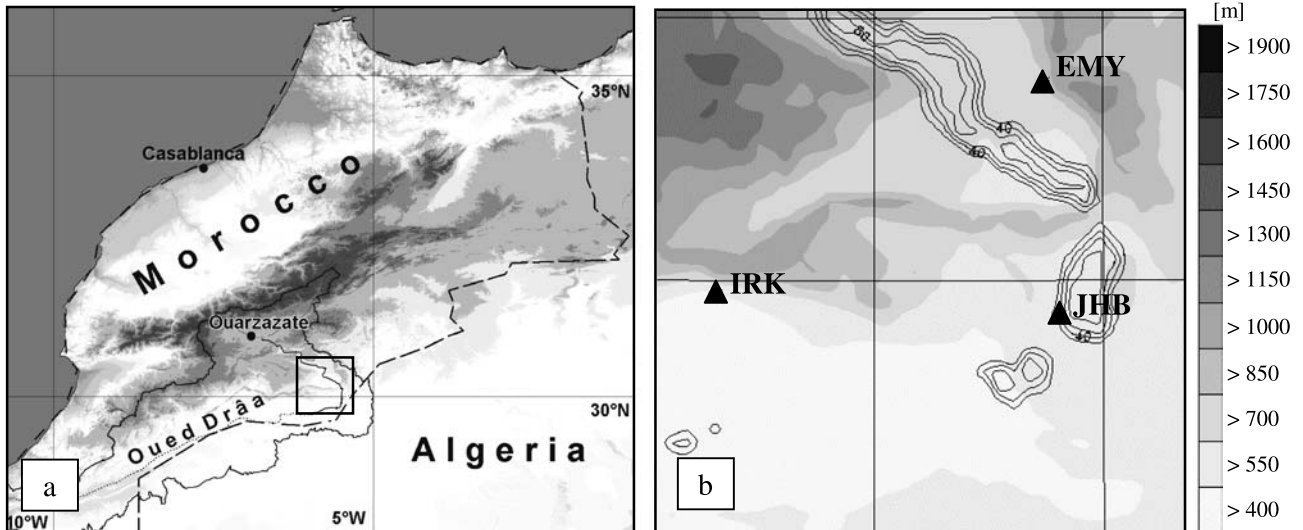


Fig. 1. (a) Location of the Drâa catchment (outlined by thin black line) and simulation area (box). (b) Smoothed topography (shaded) and vegetation cover in 20% steps of GLCC data set (isolines) for the simulation area. IMPETUS meteorological measurement stations are indicated by triangles, see Table 1 for details

Table 1. List of meteorological IMPETUS measurement stations in the simulation area

Station name	Code	Latitude	Longitude	Elevation a.s.l.
Lac Iriki	IRK	29°58'23.1" N	6°20'56.5" W	445 m
Jebel Hssain	JHB	29°56'12.12" N	5°37'43.21" W	725 m
El Miyit	EMY	30°21'49.21" N	5°37'44.4" W	792 m

references can be found in Brücher et al. (1998) and Shao et al. (2001). For this work, it is run in a non-hydrostatic mode and advection is calculated using the quasi-monotone semi-Lagrange scheme (Bermejo and Staniforth, 1992). A balance at the lower atmospheric boundary considers radiation and turbulent fluxes are determined using the Monin-Obukhov theory in the surface layer. The model uses terrain-following η -coordinates. Scalar quantities are calculated for the middle of each grid box, while advective quantities are calculated at the middle of the upstream border plain of each box. Vertical spacing of the layers is not equidistant to allow for higher resolution near the ground. The simulations presented here are realised with 20 layers, the first one with a thickness of 50 m and the upper boundary of the model at 13 km. The model is suitable for passive nesting into larger scale models as well as into itself. In this study, it is nested into LM simulations, which provide initial conditions and one-hourly atmospheric forcing at the top and the lateral boundaries of the model area. During the first hour of simulation a diastrophic phase is enabled, to gradually adjust the atmospheric state to the finer

orography of FOOT3DK. LM input fields are provided with a resolution of 0.0625° , which is approximately 7 km in the latitude of interest. The grid length used in FOOT3DK is 3 km, covering an area of $120 \text{ km} \times 120 \text{ km}$ (approximately $29^\circ 30' \text{ N}$ to $30^\circ 30' \text{ N}$ and $5^\circ 30' \text{ W}$ to $6^\circ 30' \text{ W}$, see Fig. 1). The model works with two soil layers, using the extended force-restore concept (Deardorff, 1978; Noilhan and Planton, 1989). It was further refined by Jacobsen and Heise (1982) to respond best to two forcing frequencies, which are chosen to be a diurnal and a three-hour cycle. This leads to a lower boundary of the soil model in 1 m depth. Vegetation is implemented as a single layer using the big-leaf approach.

Total evapotranspiration (E) is the sum of evaporation from the ground (E_g), re-evaporation of intercepted rainwater from plant surfaces (E_r), and plant transpiration (E_{tr}):

$$E = E_g + E_r + E_{tr} \quad (1)$$

The components on the right hand side of Eq. (1) are calculated as follows:

$$E_g = (1 - \text{veg}) \rho L_v \frac{1}{R_a} (h_u q_s(T_s) - q_1) \quad (2)$$

Table 2. Variables used in the model for calculating evapotranspiration

Variable name	Explanation	Unit
E	Total evapotranspiration	W m^{-2}
E_g	Evaporation from bare ground	W m^{-2}
E_r	Re-evaporation of intercepted rainwater from plant surfaces	W m^{-2}
E_{tr}	Transpiration	W m^{-2}
h_u	Shape parameter	–
LAI	Leaf area index	$\text{m}^2 \text{m}^{-2}$
L_v	Specific heat of evaporation	J kg^{-1}
q_s	Saturation specific humidity at the soil surface	g kg^{-1}
q_1	Specific humidity of lowest atmospheric layer	g kg^{-1}
R_a	Aerodynamic resistance	s m^{-1}
R_s	Stomatal resistance	s m^{-1}
$R_{s \text{ max}}$	Maximum stomatal resistance	s m^{-1}
$R_{s \text{ min}}$	Minimum stomatal resistance	s m^{-1}
T_s	Surface temperature	K
veg	Vegetation coverage	%
W_2	Soil moisture content in total soil layer	$\text{m}^3 \text{m}^{-3}$
W_{fl}	Field capacity of soil moisture: $W_{fl} = 0.75 W_{\text{sat}}$	$\text{m}^3 \text{m}^{-3}$
W_g	Soil moisture content in top soil layer	$\text{m}^3 \text{m}^{-3}$
W_r	Water stored on plant surfaces	kg m^{-2}
$W_{r \text{ max}}$	Maximum amount of water to be stored on plant surfaces	kg m^{-2}
W_{sat}	Saturation capacity of soil moisture	$\text{m}^3 \text{m}^{-3}$
W_{wilt}	Soil moisture at wilting point	$\text{m}^3 \text{m}^{-3}$
δ_r	Percentage of wet plant surfaces	%
ρ	Air density	kg m^{-3}

$$E_r = \text{veg} \cdot \rho L_v \frac{\delta_r}{R_a} (q_s(T_s) - q_1) \quad (3)$$

$$E_{tr} = \text{veg} \cdot \rho L_v \frac{1 - \delta_r}{R_a + R_s} (q_s(T_s) - q_1) \quad (4)$$

The factors h_u and δ_r describe the influence of soil water in the top soil layer (W_g) and stored rainwater on the plant surfaces (W_r) on E_g and E_r , respectively. They are:

$$h_u = \begin{cases} \frac{1}{2} \left(1 - \cos \left(\pi \left(\frac{W_g}{W_{fl}} \right) \right) \right) & \rightarrow W_g \leq W_{fl} \\ 1 & \rightarrow W_g > W_{fl} \end{cases} \quad (5)$$

$$\delta_r = \left(\frac{W_r}{W_{r\max}} \right)^{\frac{2}{3}} \quad (6)$$

where $W_{fl} = 0.75W_{\text{sat}}$ is the field capacity, $W_{r\max}$ is the maximum of water possibly stored on plant surfaces and W_{sat} is saturation water content of the soil.

The three constituents of evapotranspiration are determined by the potential evaporation ($q_s(T_s) - q_1$), where q_s is the saturation specific humidity at the surface (depending on surface temperature, T_s), and q_1 is the specific humidity in the lowest atmospheric layer. They also depend on the aerodynamic resistance (R_a), which comprises influences of roughness length and atmospheric stability. Transpiration (E_{tr}) additionally depends on the stomata resistance (R_s) that is calculated following Jarvis (1976) and Sellers et al. (1986).

$$R_s = \min(R_{s\max}, \frac{R_{s\min}}{\text{LAI}} F_1 F_2^{-1} F_3^{-1} F_4^{-1}) \quad (7)$$

The minimum stomata resistance ($R_{s\min}$) is plant type specific, maximum stomata resistance ($R_{s\max}$) is set uniform to 5000 s m^{-1} and LAI denotes the leaf area index. To calculate actual transpiration, minimum stomata resistance is modified by functions F_1 , F_2 , F_3 and F_4 . They represent the influences of incoming solar radiation, soil moisture content, near surface atmospheric humidity, and near surface atmospheric temperature, respectively. Only calculation of the enhanced stomata resistance due to soil moisture (F_2) is presented in detail, because this is used in our method of arti-

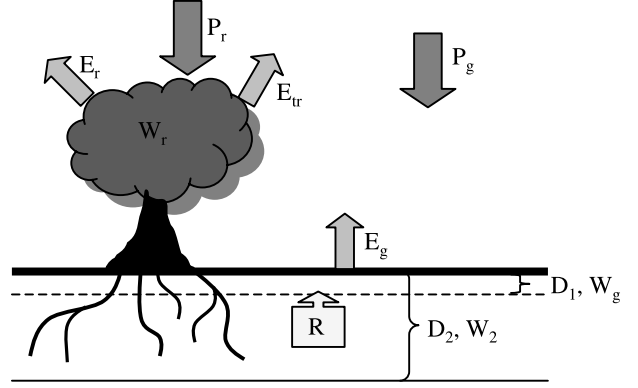


Fig. 2. Schematic sketch of quantities, relevant in the evapotranspiration calculation in the FOOT3DK model. R is the restore term, redistributing soil moisture to the top layer, D_1 and D_2 are depth of the top soil layer and the total soil, respectively

cially enhancing soil water content in some simulations:

$$F_2 = \begin{cases} 1 & \rightarrow W_2 > W_{fl} \\ \frac{W_2 - W_{\text{wilt}}}{W_{fl} - W_{\text{wilt}}} & \rightarrow W_{\text{wilt}} < W_2 < W_{fl} \\ 0 & \rightarrow W_2 \leq W_{\text{wilt}} \end{cases} \quad (E8)$$

where W_2 is the water content in the whole soil layer and W_{wilt} denotes the water capacity at the wilting point. Calculation of factors F_1 , F_3 and F_4 can be found in Dickinson et al. (1993).

Components to calculate the water budget and evapotranspiration are schematically shown in Fig. 2. Precipitation is subdivided into one portion, which falls on the ground (P_g), and one, which falls on plant surfaces (P_r). The restore term (R) stores temperature and moisture coming from the surface layer and redistributes it to the top layer, depending on vertical gradients. Further information about model physics and parameterisations can be found in Shao et al. (2001).

Surface representation is based on the global data sets ‘Global 30 Arc-Second Elevation Data Set’ (GTOPO30, orography) and ‘Global Land Cover Characterization’ (GLCC, land use). Both data sets are freely available from the U.S. Geological Survey (USGS) Earth Resources Observation System (EROS) Data Centre. The nominal horizontal resolution is $30''$ (roughly 1 km in the latitude of interest) for GTOPO30 and 1 km for GLCC. Substantially lower actual resolution of GTOPO30 for some parts of Morocco and partly inappropriate land cover coding in GLCC has to be stated.

Soil water amount and distribution for the investigated area are supplied via nesting procedure to FOOT3DK by the larger scale model LM, which is in turn nested into the global model of the DWD. For the episode simulations carried out within the framework of IMPETUS, LM is not run within a continuous analysis-forecast cycle that would allow for local soil moisture patterns to develop. Hence, soil water distributions are very coarse and tend to vary only minimal in time and space for the simulation domain. Additionally, the soil in the LM is too dry to allow any evapotranspiration, which means, that in our simulations all plants would die because they couldn't transpire. In reality, the water for the plants is provided by groundwater in deep soil layers and by irrigation. Therefore, to get a more realistic distribution of evapotranspiration in the area of interest, it is necessary to introduce some artificially created soil water distributions, based on appropriate consideration of local irrigation methods, vegetation patterns and an assumed groundwater availability.

To virtually enhance the soil water, two scenarios were performed. The first resembles irrigation by artificially setting the water storage in the top soil layer to maximum ($W_g = W_{\text{sat}}$) for the first 5 hours of simulation for all areas with vegetation cover greater 20%. We choose this setting to simulate the local irrigation practice of flooding the date palm gardens in the oasis (bordered approximately by the line of 20% vegetation cover, see Fig. 1b), when water from a 'lache' is channelled into the river oasis. This scenario will be denoted as 'irrigation' in the following. The second scenario is chosen to simulate the availability of deep groundwater to the plant roots by setting the F_2 parameter to one. This means, that there is no reduction of stomata conductance due to soil water scarcity. Thus, the plants can draw on an ideal supply of water below the lower boundary of the model, while no evaporation from bare ground will take place. This will be denoted as 'groundwater' in the following. Both scenarios represent the maximum of possible impact on evapotranspiration expected from the influences they simulate (see Chapter 4.1). The control run is performed using the soil moisture fields obtained from the LM.

The model allows to increase the resolution of the surface ($1 \text{ km} \times 1 \text{ km}$) while keeping the atmospheric grid unchanged ($3 \text{ km} \times 3 \text{ km}$). In this case surface fluxes are calculated at the finer surface resolution and then fed into the atmospheric simulations using the mosaic approach. Comparing the results of this simulation with the results obtained from simulations with the surface resolution as coarse as the atmospheric resolution ($3 \text{ km} \times 3 \text{ km}$) is used to explore the sensitivity of our model in the investigated area to represent sub-grid scale surface heterogeneity in Chapter 4.2.

A new surface data set was derived during the first IMPETUS phase from LANDSAT data (Schmidt, 2003; Schmidt and Schoettker, 2003). A preliminary version of this data set was implemented into FOOT3DK to improve the underlying land use and land cover distribution. The data set has a resolution of $28.5 \text{ m} \times 28.5 \text{ m}$ and was aggregated to $1 \text{ km} \times 1 \text{ km}$ grid boxes, with percent contributions of the different land use classes for each grid box. As not all pixels were classified, unclassified areas were filled in from the previously used GLCC data set. This is limiting the possible improvement the LANDSAT data set might give to our simulations. However, comparing the newly developed LANDSAT data with the GLCC data, substantial changes in vegetation cover and land use types are obtained and results will be shown in Chapter 4.3.

Some measured data will be presented in Chapter 4.4, to compare the simulated values with observations.

4. Results

Simulation results are presented for the period 06.06.2002 01 UTC to 07.06.2002 00 UTC. No rainfall occurred during this period and only thin high cirrus was observed in the night and morning hours.

4.1 Enhanced soil water content

First, comparisons of simulation results are shown with emphasis on soil water content. Total evapotranspiration values in W m^{-2} for 06.06.2002 12 UTC for simulations with 'irrigation' and 'groundwater' are shown in Fig. 3a and b. As pointed out in the previous

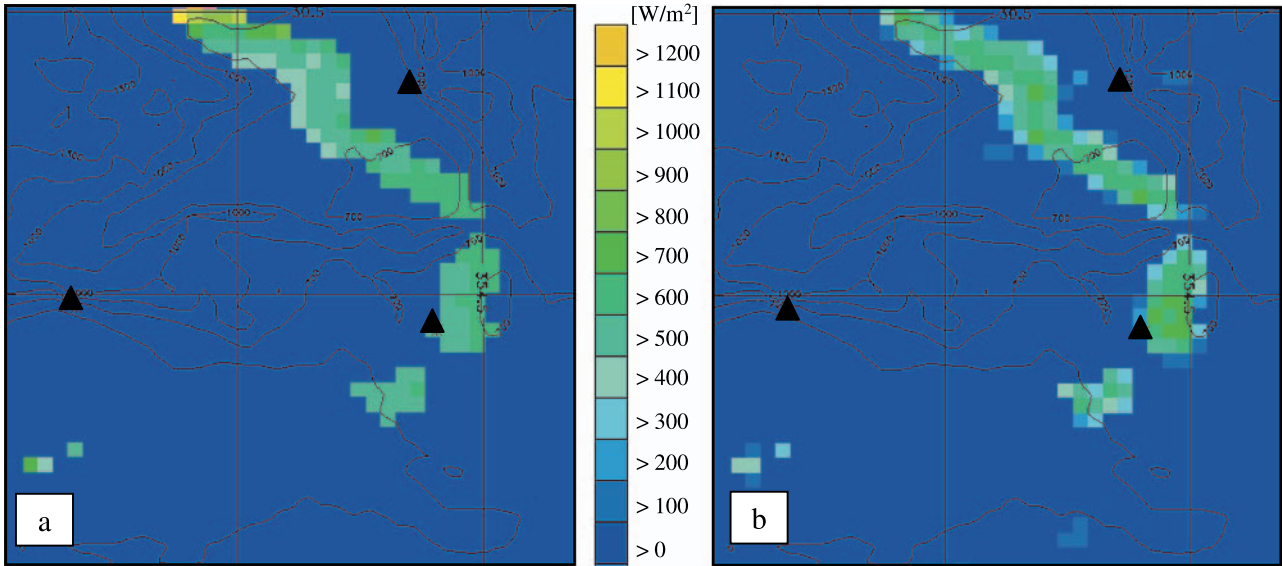


Fig. 3. Evapotranspiration [W m^{-2}] for 06.06.2002, 12 UTC, with enhanced soil moisture content for (a) ‘irrigation’ and (b) ‘groundwater’ scenario. Colour spacing is 100 [W m^{-2}]

section, values for the control run (without additional soil moisture supply) are zero for the whole area and simulation time (not shown).

While for the ‘irrigation’ run (Fig. 3a) values inside the river grove are larger than for the ‘groundwater’ run (Fig. 3b) the opposite is true outside the river oasis. This comes as no surprise since the ‘irrigation’ is only carried out for regions with vegetation cover greater than 20%, to account for the fact that only cultivated areas inside the oasis are irrigated. On the other hand, all plants even in the very sparsely vegetated exterior of the river oasis are able to draw on the ‘groundwater’. For the ‘irrigation’ run a considerable part of the total evapotranspiration is contributed from evaporation from bare ground surfaces (E_g) because of the flooding of the cultivated areas. This part of the latent heat flux subsides during the day. In the ‘groundwater’ simulation evaporation from the soil surface remains zero for the whole simulation period. Nevertheless, mean latent heat flux for the ‘groundwater’ run for the whole domain exceeds the value for the ‘irrigation’ run: Mean values for the simulation domain over 24 hours accumulate to $2.61 \cdot 10^6 \text{ J m}^{-2}$ for the ‘groundwater’ run, compared to only $2.11 \cdot 10^6 \text{ J m}^{-2}$ for the ‘irrigation’ simulation. This enhancement is clearly attributed to transpiration of plants outside the oasis (not resolved in Fig. 3).

Surface temperature (colouring) and near surface wind speed and direction (length and direction of arrows) for 15 UTC for the control run (without soil moisture enhancement, Fig. 4a) show pronounced differences to the respective fields from the run with ‘irrigation’ (Fig. 4b). Surface temperature is altered up to 12 K in some grid boxes due to evaporative cooling in the vegetated areas. Thus, changes of evapotranspiration are accompanied by changes in sensible heat flux in the same order of magnitude. Horizontal wind in the middle of the first atmospheric layer (about 25 m above ground) shows significant changes in direction and strength, especially in the vicinity of the oasis. This is attributed to enhanced static stability caused by reduced surface temperatures. The stabilisation in turn leads to a channelling effect in the near surface wind field in this area. As wind speed, air temperature, and atmospheric humidity influence transpiration (see Eq. 7), these effects might also cause alterations of evapotranspiration in areas not directly affected by the changes in soil moisture.

4.2 Sub-grid surface heterogeneity

To explore the sensitivity of the results to sub-grid surface heterogeneity, simulations are carried out on the same atmospheric grid of $3 \text{ km} \times 3 \text{ km}$ as before but a finer surface resolution

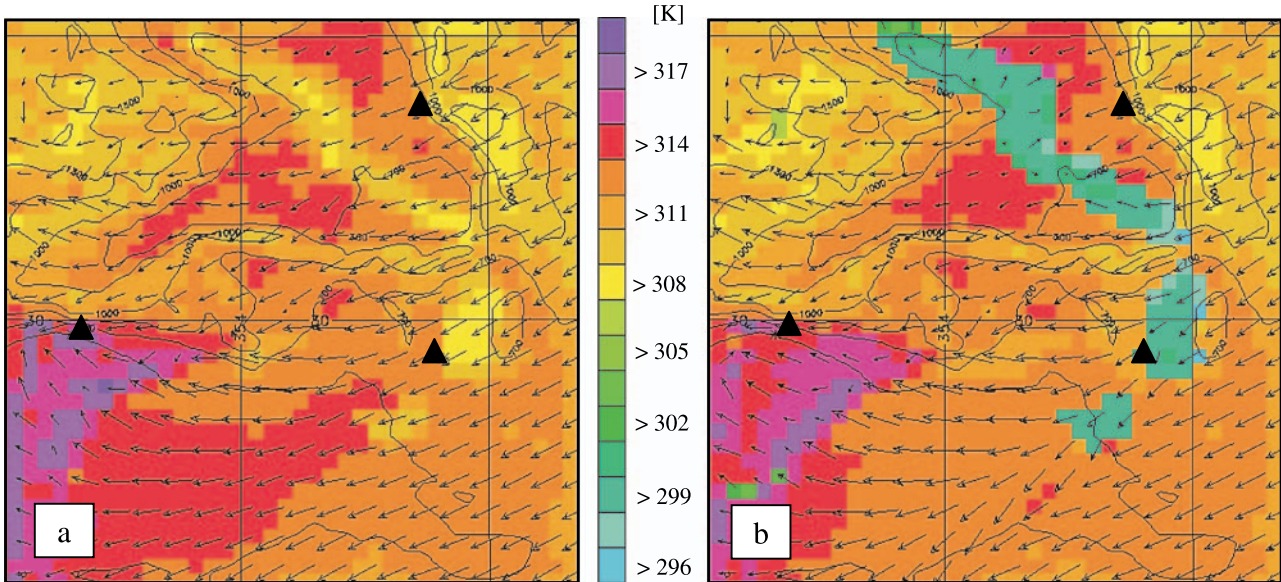


Fig. 4. Surface temperature [K] and horizontal wind (arrows) in lowest atmospheric layer, about 25 m above ground for 06.06.2002, 15 UTC, (a) without soil moisture enhancement, and (b) with ‘irrigation’. Colour spacing is 1.5 [K], max length of arrows is 8 m/s

(1 km × 1 km). As for the control run evapotranspiration is zero, this is also true for the control run with enhanced surface resolution. Noticeable differences only occur when soil moisture is enhanced.

Comparison of the ‘irrigation’ runs (Fig. 5a) for coarse minus fine surface resolution shows differences for some of the simulated grid-cells

up to 400 W m^{-2} . Mean values for the simulation area, accumulated for the whole simulation period add up to $1.84 \cdot 10^6 \text{ J m}^{-2}$ for the fine surface resolution compared to $2.11 \cdot 10^6 \text{ J m}^{-2}$ for the coarse surface grid. This reduction of latent heat flux for the finer surface resolution is also true for the ‘groundwater’ run, but for a smaller extent. Grid box values for 12 UTC differ only up to

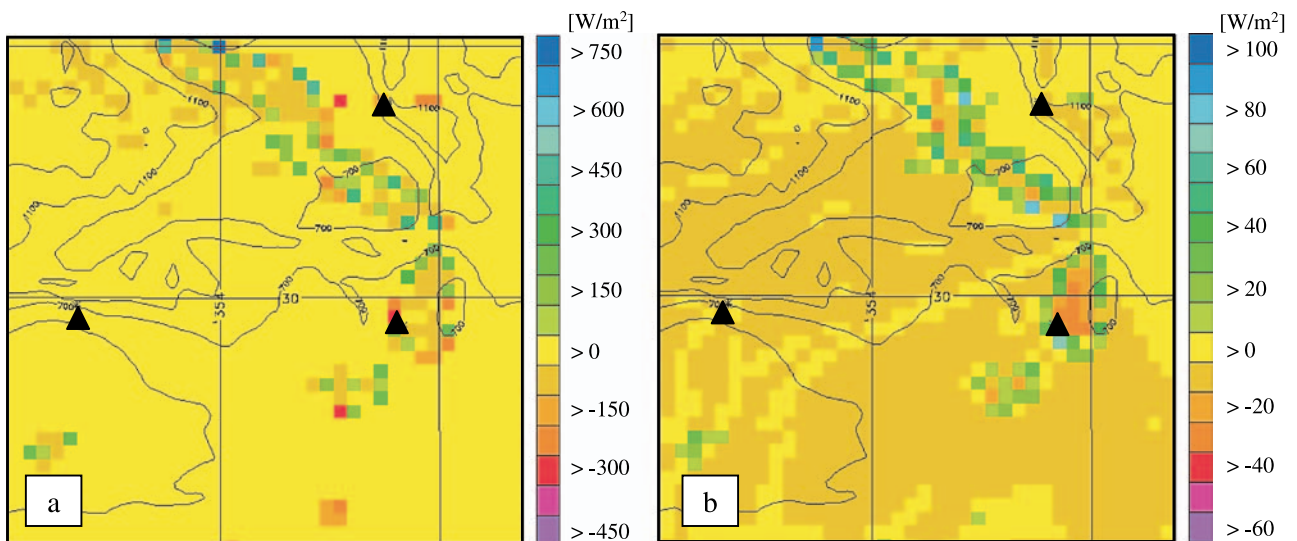


Fig. 5. Evapotranspiration differences [W m^{-2}] for 06.06.2002, 12 UTC, for (a) ‘irrigation’ and (b) ‘groundwater’ runs with coarse surface resolution minus the same simulation with fine surface resolution. Colour spacing for (a) is $75 \text{ [W m}^{-2}]$ and for (b) $10 \text{ [W m}^{-2}]$

100 W m^{-2} (Fig. 5b). Nevertheless, mean values for the entire domain accumulate to $2.54 \cdot 10^6 \text{ J m}^{-2}$ compared to $2.61 \cdot 10^6 \text{ J m}^{-2}$ for the simulation with coarse surface resolution for the investigated time.

These results depict a non-linear response of the surface fluxes (e.g. Shao et al., 2001; Hasler et al., 2002). The strong response of the ‘irrigation’ run should be viewed with caution: it is in part attributed to the fact, that the soil moisture enhancement is only carried out in areas with at least 20% of vegetation cover. The whole surface grid cell is then set to maximum soil water content. With the finer surface resolution, larger grid cells formerly bearing e.g. 20% vegetation coverage, may now split into some smaller boxes with enhanced and some boxes with reduced vegetation cover. The smaller grid boxes with less than 20% vegetation cover are therefore not ‘irrigated’. Only the remainder of the former, larger grid cell is equally ‘irrigated’ as before. In the end, there is less water distributed in the oasis in the simulation with finer surface resolution and evapotranspiration decreases. It is thus not distinguished, which part of the simulated differences is due to sub-grid surface heterogeneity and which part is due to altered soil water availabil-

ity. Even though this restriction is unsatisfying, it is inevitably part of the ‘irrigation’, in the simulation as well as in reality. For the ‘groundwater’ case, only non-linearity of simulated fluxes, induced by the strong vegetation and transpiration gradients, is regarded as source of the difference (cf. Shao et al., 2001), since water availability has not changed.

4.3 New land use/land cover data

As part of the IMPETUS project, a new land use/land cover map of the area was produced from LANDSAT data (Schmidt, 2003). Identified vegetation classes are shown in Fig. 6a in different colours. White areas are either not vegetated or not classified. To distinguish these cases, a parallel developed LANDSAT soil type data set was used to determine bare ground areas (not shown). The new data set differs considerably from the GLCC data set used before.

Vegetation cover [%] for the previously used GLCC data set is depicted in Fig. 1b. Differences LANDSAT minus GLCC data vegetation cover [%] (Fig. 6b) clearly shows, that the vegetation belt indicating the river oasis is much narrower in the new LANDSAT data set. Vegetation cover

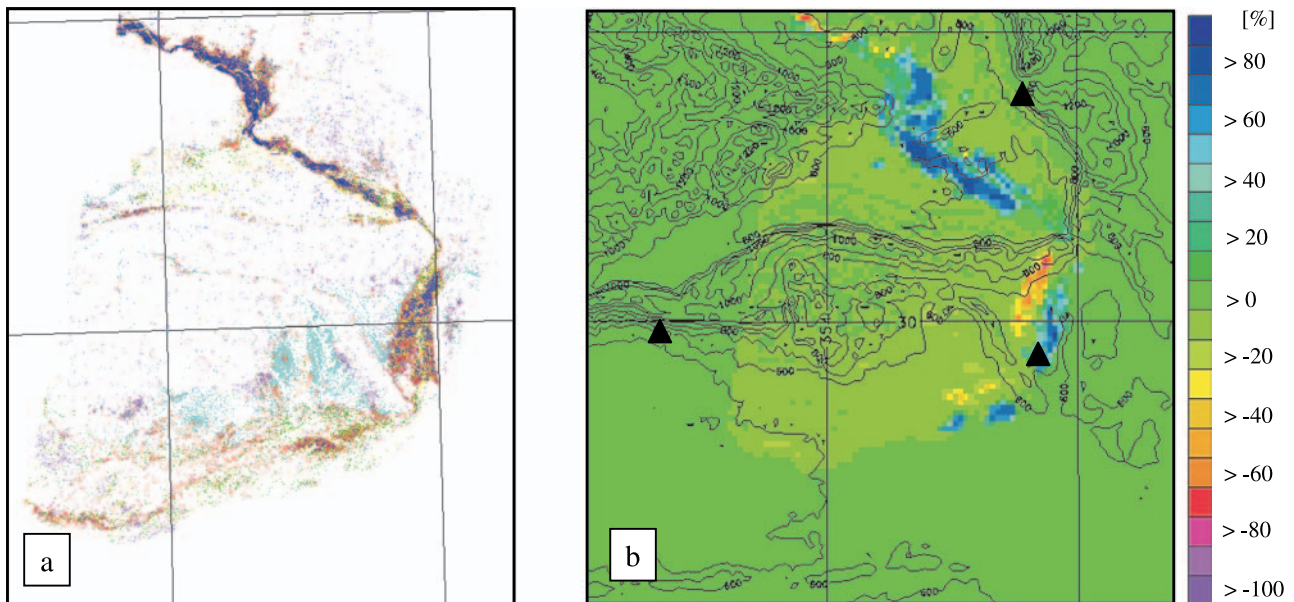


Fig. 6. (a) Land use/land cover classes with different vegetation types in LANDSAT data (blue: *Phoenix dactylifera* dense, violet: *Phoenix dactylifera* loose, red: *Zygophyllum*, green: *Tamarix aphylla*, yellow: *Tamarix africana*, cyan: *Acacia panicum*, magenta: *Acacia ziziphus*, orange: *Anabis hamada salsola*), and (b) vegetation cover difference [%] LANDSAT minus GLCC, blue (red) colours indicate reduced (enhanced) vegetation in the LANDSAT data

outside the river oasis is slightly enhanced. This might be partly due to the higher resolution of the LANDSAT data, but could also reflect land use changes occurred between taking the particular satellite images, used for the respective land use and land cover characterisation.

To take advantage of the refined surface representation, high surface resolution using the LANDSAT data set, as presented in the previous paragraph, was used for simulations. Again, additional soil moisture was implemented. Remarkable differences show up when simulation results for identical runs with different underlying land use/land cover data sets are compared. The simulations with ‘irrigation’ (Fig. 7a) as well as the ones with ‘groundwater’ (Fig. 7b) show reduced mean evapotranspiration values for 12 UTC when realised with the LANDSAT data. Reduced vegetation in the river oasis in this data set leads to reduced evapotranspiration values in the concerned area.

However, differences for the ‘groundwater’ run are smaller than for the ‘irrigation’ run. Accumulating the area mean latent heat flux values for the whole simulation period obtained from the ‘irrigation’ run add up to $1.59 \cdot 10^6 \text{ J m}^{-2}$. This is a reduction of $0.25 \cdot 10^6 \text{ J m}^{-2}$ compared to the respective value for the simulation using the GLCC data set and fine surface resolution. On the other hand, mean values for the ‘groundwater’ run accumulate to $2.39 \cdot 10^6 \text{ J m}^{-2}$, depicting a reduction of $0.15 \cdot 10^6 \text{ J m}^{-2}$ compared to the ‘groundwater’ scenario and fine surface resolution with the GLCC data set. The reason for the less pronounced reduction in the ‘groundwater’ run is transpiration of plants outside the river oasis. There, vegetation cover is enhanced in the LANDSAT data set, diminishing the effect of reduced vegetation in the oasis (Fig. 6b). In Table 3 accumulated latent heat flux values for different simulations are listed to allow a better overview.

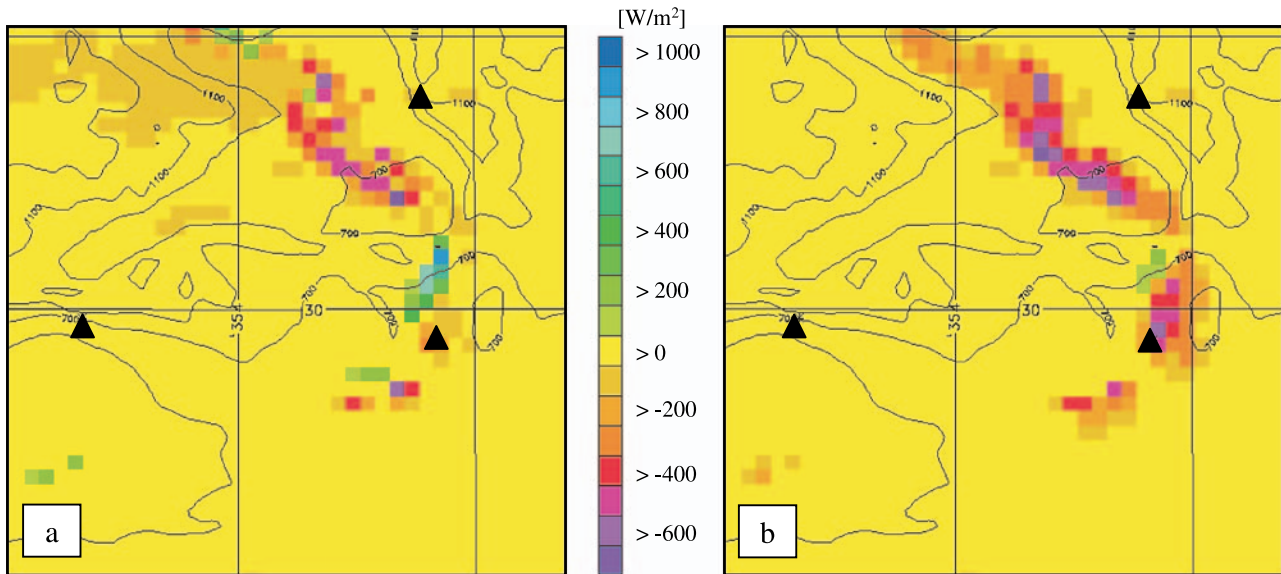


Fig. 7. Differences of evapotranspiration in $[\text{W m}^{-2}]$ for 06.06.2002, 12 UTC, GLCC minus LANDSAT data set use in (a) ‘irrigation’ and (b) ‘groundwater’ scenario. Colour spacing is $100 [\text{W m}^{-2}]$

Table 3. Mean evapotranspiration for the investigated area, accumulated over 24 hours for realisations with different underlying data sets

‘Irrigation’ scenario J m^{-2}	‘Groundwater’ scenario J m^{-2}	Surface data set
2.11	2.61	GLCC data, coarse resolution
1.84	2.54	GLCC data, fine resolution
1.59	2.39	LANDSAT data, fine resolution

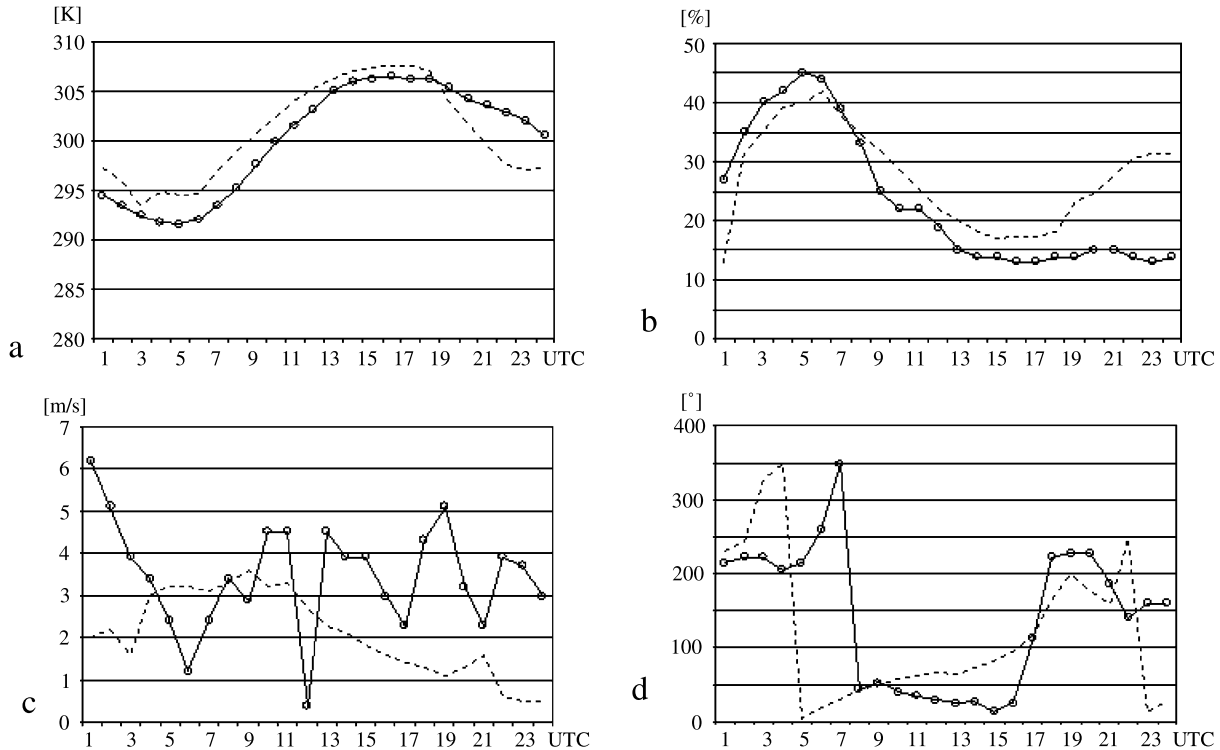


Fig. 8. Measurements for station Jebel H'ssain (JHB), 06.06.2002, 00 UTC–24 UTC (continuous line with open circles), compared to simulations with ‘groundwater’ and LANDSAT data (dashed line) for (a) temperature [K], (b) relative humidity [%], (c) wind speed [m/s], and (d) wind direction [°]

4.4 Comparison with measured data

Within the scope of the IMPETUS project, ground measurements of meteorological parameters were taken at several sites in the Drâa catchment. Three of these sites are located in the area of interest and their location is marked by black triangles in Fig. 1b. For one of these stations (Jebel H'ssain, JHB) comparison of measured variables with simulated grid box values are presented in Fig. 8. For the other stations results are similar.

Even for the simulation without soil moisture enhancement, all simulation results show similar characteristics at the measurement sites. For this reason, the observations (continuous line with open circles) are only compared with the LANDSAT ‘groundwater’ run, which should be regarded as typical for all runs. Differences for the first hour of simulation are likely to be caused by the *diastrophic* phase used to adjust the LM fields to the finer resolved FOOT3DK orography.

Near surface temperature is slightly overestimated for the first 19 hours of the simulation. Thereafter, an underestimation occurs in the

early night hours at the end of the simulation (Fig. 8a). Relative humidity is well depicted for the first night and during the day, but is overestimated in all runs for the second night (Fig. 8b). This is partly explained by an underestimation of near surface temperature for this time (Fig. 8a), but we assume, that it is mainly caused by excess advection of moister air from northern directions (Fig. 8d) obtained from the forcing LM run. Wind speed comparisons of simulated and measured values (Fig. 8c) yield the same order of magnitude. The diurnal cycle in wind direction (Fig. 8d) is represented fairly good. During the last hours of the simulation, northerly to northeasterly winds are simulated instead of the measured southeasterly directions. This may have caused the underestimation of temperature and overestimation of relative humidity as northerly winds advect air from the Atlas mountains, whereas southerly winds advect air from the Saharan desert. To interpret the simulation results with respect to measured values (Fig. 8) one should keep in mind, that point measurements are compared with simulated values for a

3 km × 3 km atmospheric grid-cell. These values are linearly interpolated to a height 2 m above ground (the simulated values for the lowest atmospheric layer are calculated for about 25 m above ground). Since the point measurements are strongly influenced by local effects, they may not be representative for the whole grid box.

Meteorological measurements for the simulated day are only available for sites relatively far from the river oasis. As simulated evapotranspiration differs most in the vegetated areas in the oasis, the sparsely vegetated grid boxes containing the measurement sites show only small variability. Nevertheless, the simulations can be considered as capable to represent the general features (e.g. diurnal cycle of wind directions, with colder air coming down from the elevated regions in the northern part of the area during night hours and warmer air protruding into the simulation domain from south during daytime).

As further part of the IMPETUS framework, transpiration of several representative plants at the site El Miyit (EMY) and of date palms in the oasis is measured for some days in spring and autumn. Transpiration was measured as kilograms of transpired water per square meter leaf area per day. The values obtained from leaf measurements are upscaled to area-covering values by estimating leaf area index of the respective plants and counting the number of this species for the area (personal communication with Gresens, 2003). In order to compare the measured transpiration with simulated contributions of model transpiration to accumulated latent heat fluxes, measurements are scaled with a constant value of L_v , the specific heat of evaporation.

Measured values for the EMY site are ranging from $0.012 \cdot 10^6 \text{ J m}^{-2}$ to $0.14 \cdot 10^6 \text{ J m}^{-2}$ per day. The remarkable differences of more than one order of magnitude in the observations are due to varying leaf area index as well as to varying soil water scarcity, steering the stomatal resistance. Simulated transpiration for the corresponding grid box is zero for simulations without soil moisture enhancement and with ‘irrigation’ (since the grid box is located outside the oasis and therefore not irrigated) and about $1.3 \cdot 10^6 \text{ J m}^{-2}$ for ‘groundwater’ simulations. Overestimation of transpiration for the grid-cell containing the EMY measurement site is partly caused by too high leaf area in the model (about

$0.36 \text{ m}^2 \text{ m}^{-2}$ in the model, compared to $0.03\text{--}0.11 \text{ m}^2 \text{ m}^{-2}$ in the measurements for different days). While measured values of $0.012 \cdot 10^6 \text{ J m}^{-2}$ can be considered as nearly zero, this is not the case for a value of $0.14 \cdot 10^6 \text{ J m}^{-2}$. Assuming 12 hours of constant transpiration during a day, the former value would result in latent heat fluxes well below 5 W m^{-2} , which is less than the accuracy that can possibly be expected from the model. The latter value, on the other hand, would under the same assumption produce latent heat fluxes of more than 100 W m^{-2} , which is well in the predictable range.

Besides the measurements at the test site EMY, transpiration was additionally measured at a date palm in the oasis, which was not only irrigated using the ‘laché’, but also with water from a groundwater pump. In this case, transpiration values accumulate to $4.79 \cdot 10^6 \text{ J m}^{-2}$ for a whole day. This can be regarded as a maximum value of real date palm transpiration. Simulated evapotranspiration values for a randomly chosen grid-cell inside the oasis lead to values between zero (without soil moisture enhancement), $9.29 \cdot 10^6 \text{ J m}^{-2}$ for ‘groundwater’, and about $16.85 \cdot 10^6 \text{ J m}^{-2}$ for ‘irrigation’ simulations. The simulated overestimation of transpiration must partly be attributed to overestimation of leaf area index for date palms by a factor of 3.75 ($4.4 \text{ m}^2 \text{ m}^{-2}$ in the model instead of observed $1.2 \text{ m}^2 \text{ m}^{-2}$). Taking this into account we can conclude that simulated values capture the observations quite well.

5. Discussion

In semi-arid regions, soil water availability is the main restriction for evapotranspiration (cf. e.g. Taylor et al., 1997), but normally information about amount and distribution of this quantity is poor. Therefore, different approaches are used to enhance the quality of simulated surface energy distributions by artificially introducing soil moisture fields. Braun et al. (2001) improve simulation results by artificially enhancing soil moisture content by 50% or 100%, for their research site, but receive reduced accuracy in representation of boundary layer properties. Using a different approach, we introduced artificial soil moisture fields trying to resemble the processes of groundwater below the lower

boundary of the model and irrigation practice. As no measurements apart from surface stations are available in our study we cannot discuss the accuracy of simulations presented here for boundary layer properties. But artificially enhanced soil moisture and associated surface energy balance noticeably affect near surface wind fields with reasonable results. We show, that model sensitivity to vegetation cover and leaf area index as reported by Brotzge and Weber (2002) only show up under conditions of enhanced soil moisture in our simulations.

We find a non-linear reaction of evapotranspiration to surface properties as reported e.g. by Shao et al. (2001). As expected, the aggregation effect due to non-linearity of the simulated surface energy fluxes leads to enhanced latent heat fluxes in the runs with coarser surface resolution. At the vegetation border, effects of neighbouring grid boxes with different land use/land cover types can influence simulation results, as pointed out by Hasler et al. (2002). These effects can be seen in differences of evapotranspiration with and without enhanced surface resolution.

Simulations using artificially enhanced soil moisture capture observed transpiration values for the oasis quite well. For the area outside the oasis, transpiration is overestimated, but as absolute values are small, this only marginally reduces simulation accuracy. Improvements of the results are expected from reduction of leaf area index to measured amounts. Comparison of observed meteorological values for the measurement sites show no significant differences between the realised simulations with respect to agreement with observational data. This should be attributed to the sparse vegetation in the grid boxes outside the oasis, inhibiting noticeable reactions of meteorological fields to enhanced transpiration. It is, therefore, necessary to compare the simulation results also with meteorological measurements in the river oasis, which is more sensitive to the implemented changes. For future simulations of more recent episodes, some meteorological observations in the river oasis will be available from newly begun IMPETUS measurements.

Besides the probability that the measurements may not be representative for the simulated grid box (cf. Noilhan et al., 1991), upscaling transpiration measurements from single leaves to area

values is very difficult. So we also have to cope with a significant level of uncertainty in the measured values (cf. Infante et al., 1997).

6. Conclusions

In this study, a mesoscale atmospheric model with a relatively simple Soil-Vegetation-Atmosphere Transfer (SVAT) scheme is used to simulate evapotranspiration under conditions of semi-arid climate, sparse vegetation, and very limited data availability. In semi-arid regions soil moisture is usually the limiting factor for evapotranspiration. To improve evapotranspiration simulation, three problems have to be dealt with:

- Soil moisture obtained from the driving model (LM) is too low to allow the plants to transpire
- Measurements of soil moisture distributions are not available
- The soil part of the meteorological model contains only two layers and the lower boundary is at a depth of 1 m below the surface

For these reasons, soil moisture is artificially enhanced, using sensible assumptions on soil water distribution in the region.

- A so called ‘groundwater’ scheme is invented to overcome the problems of deep rooting plants, drawing water from the soil well below the lower boundary of the model
- A so called ‘irrigation’ scheme is implemented to resemble the local irrigation practise (flooding of cultivated areas)

The procedures to artificially enhance soil moisture realised in this work prove to be a possible way to produce maximum evapotranspiration in the region. The presented types of soil moisture enhancement are able to cope with the above-mentioned shortcomings of the model and input data, which are typical problems for meteorological simulations in semi-arid data-sparse regions.

Findings of previous works (e.g. Shao et al., 2001) concerning the influence of sub-grid scale surface heterogeneity on simulated partitioning of sensible and latent heat fluxes are confirmed for a semi-arid area.

A new land use/land cover data set for the catchment, obtained from LANDSAT data is presented. Comparison to the previously used USGS

GLCC data set shows remarkable differences in extent and distribution of the vegetation. Even though, vegetation in both data sets is quite small, differences in surface energy flux partitioning is not negligible. Therefore, for this region a revised land use/land cover data set would be of importance for future investigations.

We conclude, that even with its relatively simple SVAT scheme, the model is capable to reproduce realistic and consistent fields of evapotranspiration and related quantities for the research area, when some simple assumptions on soil water availability are implemented.

Acknowledgement

This work was supported by the Federal German Ministry of Education and Research (BMBF) under grant No. 01 LW 0301A and by the Ministry of Science and Research (MWF) of the federal state of Northrhine-Westfalia under grant No. 223-21200200. We wish to especially thank Dipl.-Ing.Agr.F. Gresens (Institut für Pflanzenernährung, University Bonn, Germany) for his measurement results, even though they were still in an experimental state and are yet unpublished.

References

- Barmejo R, Staniforth A (1992) The conversion of semi-lagrangian advection schemes to quasi-monotone schemes. *Mon Wea Rev* 120: 716–729
- Braun P, Maurer B, Müller G, Gross P, Heinemann G, Simmer C (2001) An integrated approach for the determination of regional evapotranspiration using mesoscale modelling, remote sensing and boundary layer measurements. *Meteorol Atmos Phys* 76: 83–105
- Brotzge JA, Weber D (2002) Land-surface scheme validation using the Oklahoma Atmospheric Surface-layer Instrumentation System (OASIS) and Oklahoma Mesonet data: Preliminary results. *Meteorol Atmos Phys* 80: 189–206
- Brücher W, Kerschgens MJ, Martens R, Thielen H, Massmeyer K (1998) Tracer experiments in the Freiburg-Schauinsland area – Comparison with flow and dispersion models. *Meteor Z*, NF 7: 32–35
- Bullock P, Le Houérou H (1996) Land degradation and desertification, ch 4. In: Watson RT, Zinyowera RT, Moss MC, Dokken RH (eds) *Climate change 1995: impacts adaptations and mitigation of climate change: scientific-technical analyses*. Cambridge: Cambridge University Press, pp 171–189
- Deardorff JW (1978) Efficient prediction of ground surface temperature and moisture, with inclusion of a layer of vegetation. *J Climate* 1: 1086–1097
- Dickinson RE, Henderson-Sellers A, Kennedy PJ (1993) *Biosphere-Atmosphere Transfer Scheme (BATS) Version 1e* as coupled to the NCAR Community Climate Model, NCAR Tech Note, TN275 + STR
- Finckh M, Staudinger M (2002) Mikro- und makroskalige Ansätze einer Vegetationsgliederung des Drâa-Einzugsgebietes (Südmorokko). *Berichte der Reinhold-Tüxen-Gesellschaft* 14: 81–92 (in german)
- Gleick PH (1992) Effects of climate change on shared freshwater resources, ch 9. In: Mintzer IM (ed) *Confronting climate change: risks, implications and responses*. Cambridge: Cambridge University Press, pp 127–140
- Hasler N, Iorgulescu I, Martilli A, Liston GE, Schlaepfer R (2002) Local climate and water availability changes due to landscape modifications: A numerical experiment over southeastern Spain. In: Beniston M (ed) *Climatic change: Implications for the hydrological cycle and for water management*. Dordrecht, New York: Kluwer Academic Publishers, pp 301–328
- Hulme M (1992) Rainfall changes in Africa: 1931–1969 to 1961–1990. *Int J Climatol* 12: 685–699
- Infante JM, Rambal S, Joffre R (1997) Modelling transpiration in holm-oak savannah: scaling up from the leaf to the tree scale. *Agric Forest Meteorol* 87: 273–289
- Jacobsen I, Heise E (1982) A new economic method for the computation of the surface temperature in numerical models. *Beitr Phys Atmosph* 55: 128–141
- Jarvis PG (1976) The interpretations in the variations in leaf water potential and stomatal conductance found in canopies in the field. *Philos Trans R Soc London, Ser B* 273: 593–610
- Kite GW, Droogers P (2000) Comparing evapotranspiration estimates from satellites, hydrological models and field data. *J Hydrol* 229: 3–18
- Kustas WP, Goodrich DC, Moran MS, Amer SA, Bach LB, Blanford JH, Chehbouni A, Claassen H, Clements WE, Doraiswamy PC, Dubois P, Clarke TR, Daughtry CST, Gellman DI, Grant TA, Hipps LE, Hiete AR, Hulmes KS, Jackson TJ, Keefer TO, Nichols WD, Parry R, Perry EM, Pinker RT, Pinter PJ Jr, Qi J, Riggs AC, Schmugge TJ, Shutko AM, Stannard DI, Swiatek E, van Leeuwen JD, van Zyl J, Vidal A, Washburne J, Weltz MA (1991) An interdisciplinary field study of the energy and water fluxes in the atmosphere-biosphere system over semiarid rangelands: description and some preliminary results. *Bull Amer Meteor Soc* 72: 1683–1705
- Le Houérou HN, Hoste CH (1977) Rangeland production and annual rainfall relations in the Mediterranean Basin and in the African Sahelo-Sudan zone. *J Range Management* 30: 181–189
- Noilhan J, Lacarrere P, Bougeault P (1991) An experiment with an advanced surface parameterization in a meso-B model. Part III: Comparison with the HAPEX-MOBILHY data set. *Mon Wea Rev* 119: 2392–2413
- Noilhan J, Planton S (1989) A simple parameterization of land surface processes for meteorological models. *Mon Wea Rev* 117: 536–549
- Parish R, Funnell DC (1999) Climate change in mountain regions: some possible consequences in the Moroccan High Atlas. *Glob Environ Change* 9: 45–58

Simulating evapotranspiration in a semi-arid environment

- Schmidt M (2003) Development of a fuzzy expert system for detailed land cover mapping the Drâa catchment (Morocco) using high resolution satellite images. PhD thesis, at the University of Bonn, Germany
- Schmidt M, Schoettker B (2003) Sub-pixel analysis in combination with knowledge based decision rules to optimise a land cover classification. Proceedings of the EARSeL Symposium 2003 in Gent, Belgium
- Sellers PJ, Mintz Y, Sud YC, Dalcher A (1986) A simple biosphere model (SiB) for use within general circulation models. *J Atmos Sci* 43: 505–531
- Shao Y, Sogalla M, Kerschgens M, Brücher W (2001) Effects of land surface heterogeneity upon surface fluxes and turbulent conditions. *Meteorol Atmos Phys* 78: 157–181
- Solh M, Amri A, Ngaido T, Valkoun J (2001) Policy and education reform needs for conservation of dryland biodiversity. *J Arid Environ* 54: 5–13
- Taylor CM, Harding RJ, Thorpe AJ, Bessemoulin P (1997) A mesoscale simulation of land surface heterogeneity from HAPEX-Sahel. *J Hydrol* 188–189: 1040–1066

Authors' addresses: H. Hübener, Institute of Geophysics and Meteorology, University of Cologne, Germany (e-mail: huebener@meteo.uni-koeln.de); M. Schmidt, CSIRO Earth Observation Center, GPO BOX 3023, 2601 Canberra, ACT, Australia; M. Sogalla, Institute of Geophysics and Meteorology, University of Cologne, Germany; M. Kerschgens, Institute of Geophysics and Meteorology, University of Cologne, Germany.